

## Article

# Analysing Airflow Velocity in the Canopy to Improve Droplet Deposition for Air-Assisted Spraying: A Case Study on Pears

Rongkai Shi <sup>1</sup>, Hao Sun <sup>1</sup>, Wei Qiu <sup>1,\*</sup> , Xiaolan Lv <sup>2</sup>, Fiaz Ahmad <sup>3</sup> , Jiabing Gu <sup>1</sup>, Hongfeng Yu <sup>1</sup> and Zhengwei Zhang <sup>1</sup>

<sup>1</sup> Key Laboratory of Intelligent Equipment for Agriculture of Jiangsu Province, College of Engineering, Nanjing Agricultural University, Nanjing 210031, China

<sup>2</sup> Institute of Agricultural Facilities and Equipment, Jiangsu Academy of Agricultural Sciences, Nanjing 210014, China

<sup>3</sup> Department of Agricultural Engineering, Bahauddin Zakariya University, Multan 60800, Pakistan

\* Correspondence: qiuwei@njau.edu.cn; Tel.: +86-158-5072-4893

**Abstract:** The suitability of airflow velocity in airborne spraying operations in orchards is mostly evaluated on the basis of inlet and outlet based on the airflow velocity at the canopy. However, the airflow velocity required to penetrate into the inner layer of the canopy, which is prone to pests and diseases, is still unclear due to variation in the geometry of the plant canopies. In this study, pear trees were selected as an example to explore the variations in the law of airflow attenuation in the inner canopy. Furthermore, we examine mist droplet formation in the inner canopy to determine a suitable inner canopy airflow end velocity (ICAEV) for air-assisted application. We also conducted a field validation test. The results showed that the majority of airflow velocity loss occurred in the middle and outer part of the canopy; rapid decline of airflow occurred in the 0–0.3 m section, whereas the slow decline of airflow occurred in the 0.3–0.8 m section. When the ICAEV is in the range of 2.70–3.18 m/s, the spraying effect is better. The droplet deposition variation coefficient was 42.25% compared with 51.25% in the conventional airflow delivery mode. Additionally, the droplet drift was reduced by 12.59  $\mu\text{g}/\text{cm}^2$ . The results of this study can identify a suitable ICAEV for air-assisted spraying in orchards.

**Keywords:** air-assisted spraying; canopy; wind demand criteria; spraying effectiveness



**Citation:** Shi, R.; Sun, H.; Qiu, W.; Lv, X.; Ahmad, F.; Gu, J.; Yu, H.; Zhang, Z. Analysing Airflow Velocity in the Canopy to Improve Droplet Deposition for Air-Assisted Spraying: A Case Study on Pears. *Agronomy* **2022**, *12*, 2424. <https://doi.org/10.3390/agronomy12102424>

Academic Editor: Andrea Sciarretta

Received: 18 August 2022

Accepted: 4 October 2022

Published: 6 October 2022

**Publisher's Note:** MDPI stays neutral with regard to jurisdictional claims in published maps and institutional affiliations.



**Copyright:** © 2022 by the authors. Licensee MDPI, Basel, Switzerland. This article is an open access article distributed under the terms and conditions of the Creative Commons Attribution (CC BY) license (<https://creativecommons.org/licenses/by/4.0/>).

## 1. Introduction

Orchard pest and disease control is an important part of orchard production development [1,2], and implementing effective scientific control measures can effectively reduce the loss of orchard crops. However, due to the increasing scale of agricultural production, problems such as uneven application, wasteful use of pesticides, and environmental pollution are becoming ever more prominent [3,4], and the frequent application of pesticides can have an impact on land ecology.

Air-assisted spray technology can enhance application by disturbing branches and leaves through auxiliary airflow, promoting the deposition of droplets on crops, and simultaneously expanding the canopy range that droplets can reach and driving droplets to interact with branches and leaves in the canopy [5,6]. Based on the varying characteristics of different fruit tree species or individual species at different growth stages, researchers have changed the trajectory of airflow and spray during transport in order to enhance application. This has led to the design of a variety of sprayers with different designs and functions. For example, air-assisted tunnel sprayers [7] use two rows of air-assisted tunnels for droplet transport and recovery. Crawler-type multi-channel air-assisted orchard sprayers [8] achieve high rates of droplet penetration and reduce drift by adjusting the air outlet channels. Tower orchard sprayers [9] achieve full coverage of their target through the height arrangement of their own fans. Freyr drone sprayers [10] achieve efficient and

uniform application on large-scale farms using precise GPS positioning. In recent years, researchers have noted the effects of canopy density and width on airflow distribution. For example, Hong et al. [11] predicted the velocity distribution inside and around the crown by establishing a comprehensive CFD model and compared it with the actual measurement. However, the discussion of airflow field distribution lacks in-depth analysis of the airflow attenuation characteristics and the generalised law based on wind demand characteristics inside the canopy. Some researchers have investigated the porosity of target canopies [12] and canopy closure [13,14], and they proposed the airflow penetration model and also conducted experimental validation. Meanwhile, by using the porous medium model [15,16] and the simplified equivalent porous medium model [17], we studied the influence of canopy morphology and leaf density on the airflow field and simulated the complex process of droplet transportation by airflow coercion.

The field has transitioned from focusing on machine features to machine–craft fusion with a focus on canopy characteristics, as well as the influence and requirements of the canopy on the distribution of the airflow field. However, most studies are currently on flow field analysis under “no canopy conditions” [18,19] or on flow field analysis outside the canopy with a “canopy obstacle” [20,21]. The airflow motion of air-assisted spray in orchards consists of two parts: the inner and outer canopy. The outer canopy airflow motion satisfies the free jet theory, and the axial airflow decays exponentially with increasing distance, which is inversely related to the jet outlet width and initial velocity [22], with high exit airflow velocity and fast decay [23,24]. Compared with the decay of airflow outside the canopy, the airflow decay pattern inside the canopy is not clear. When the airflow passes through the canopy, its energy must change, affecting the distribution of droplets deposited in the canopy. Therefore, it is important to pay attention to the wind demand inside the canopy, clarify the decay law of airflow therein, and explore the ICAEV for suitable droplet deposition to further improve application and reduce the amount of liquid spray required.

This study used pear trees (variety: Crown) as the model species, and aimed to achieve the following: (1) to measure the distribution of inner canopy airflow velocity under different conditions to clarify the change in attenuation of airflow at different positions in the canopy; (2) to compare and analyse droplet deposition and coverage with different ICAEVs, to determine a suitable ICAEV for pear trees, and to verify this by conducting a field trial. The purpose of this study is to identify suitable ICAEVs for fruit trees specifically for air-assisted plant protection, and to provide a new reference for air-assisted spraying research in orchards.

## 2. Materials and Methods

### 2.1. Experimental Preparation

#### 2.1.1. Experimental Apparatus

The experimental device, a three-dimensional mobile air-assisted spraying platform (Figure 1), mainly consisted of the following systems: walking (fixed walking speed 1 m/s), lifting and adjusting, air supply, and sprayer. The walking system was composed of batteries, a controller, a motor, handles, and a universal wheel. The lifting and regulating system was composed of an electric lifting platform and a three-axis module. The adjustable height of the electric lifting platform was 0.42–2 m and the effective range of the three-axis module's  $x$ -axis (walking direction),  $y$ -axis (wind direction), and  $z$ -axis (vertical direction) were 0–1, 0–1, and 0–1.2 m, respectively. The air supply system was made of an invertible electric duct fan (260 mm diameter; 1080 m<sup>3</sup>/h airflow; 3200 r/min rated speed), which was used as the air supply system, mounted on the three-axis module slider. The sprayer system mainly consisted of a pesticide tank (40 L), pipes, a piston pump, and a spray conical nozzle (QY15; spray angle: 110°; spray pressure: 0–1.5 MPa). The experimental device can be used to do the following things: (1) provide airflow at different speeds to explore the airflow velocity distribution in the canopy; (2) study the effect of different ICAEVs on the droplet deposition distribution.

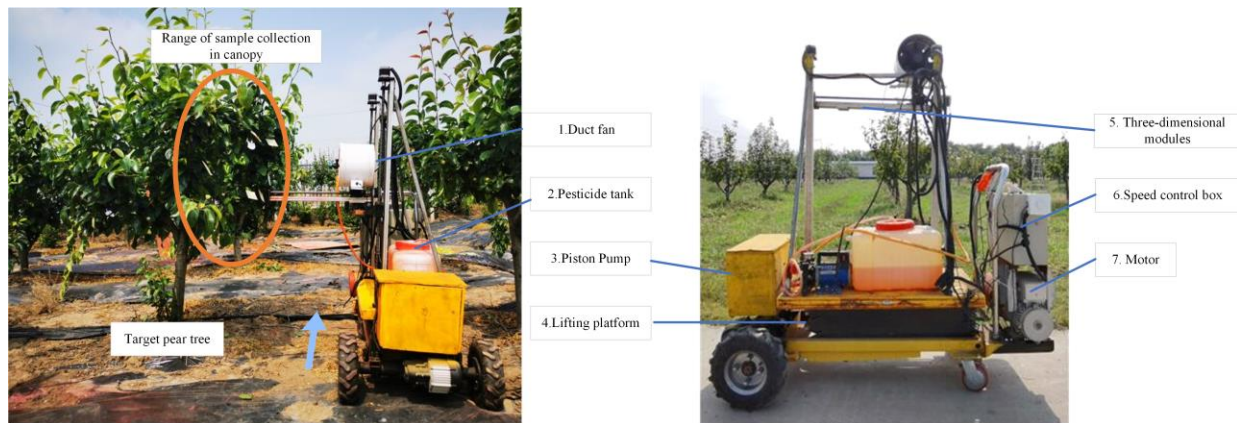


**Figure 1.** Three-dimensional mobile air-assisted spray platform.

The crawler-type multi-channel orchard air spray is mainly used to verify whether the ICAEV is reasonable. By independently adjusting the airflow velocity at each airflow outlet, the airflow velocity reaching each area of the canopy is controlled. The crawler-type multi-channel orchard air-assisted sprayer mainly consisted of a track chassis, an air supply system, and a sprayer system. The crawler chassis mainly consisted of an engine, a travel system, and a steering system. The air supply system included an axial fan, a governor, an inverter, and batteries. The sprayer system mainly consisted of a pesticide tank (400 L), a piston pump, a four-way distribution valve, a pressure gauge, a regulating valve, application pipes, return pipes, and a conical spray nozzle (QY15; spray angle:  $110^\circ$ ; spray pressure: 0–1.5 MPa). In order to achieve differential airflow at each outlet, a frequency-convertible electrically driven duct fan was added to the outlet to achieve non-uniform air-assisted application, as shown in Figure 2b.

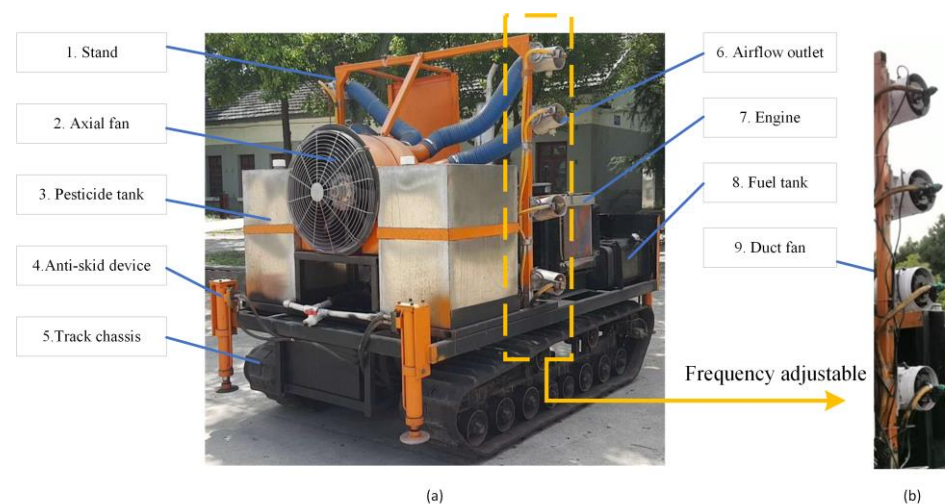


**Figure 2.** Crawler-type multi-channel orchard air-assisted sprayer. (a) Structure display of Crawler-type multi-channel orchard air-assisted sprayer. (b) Layout of four duct fans.

### 2.1.2. Experimental Conditions

The experiment was conducted on 7–9 May 2022, at the Family Farm of Sisi Yu, Pancheng Street, Pukou District, Nanjing, China ( $118.42^\circ$  E longitude,  $32.98^\circ$  N latitude), and the ambient wind velocity, temperature, and relative humidity were measured with a TSI9545 hot-wire anemometer (TSI Inc., Shoreview, MN, USA) and a hygrometer (Zhejiang, China), as shown in Table 1. To obtain reliable data, the weather conditions at the site were monitored at the end of a single experimental measurement, and measurements were discontinued until the natural airflow velocity was  $<1$  m/s.

**Table 1.** Weather conditions during spraying.

Date	Air Temperature (°C)		Natural Wind Velocity (Magnitude)	Relative Humidity (%)
	Minimum	Maximum		
7 May 2022	18	29	East wind, <2	80
8 May 2022	17	29	East wind, <2	79
9 May 2022	19	29	East wind, <2	82

**2.2. Measurement of Inner Canopy Airflow Velocity in the Field under Different Conditions**

Five pear trees of similar growth stage, i.e., a leaf area density  $L_r$  of approximately  $5.20 \text{ m}^2/\text{m}^3$ , with an average stem height of 2.08 m and an age of approximately 5 years, were selected for the field trial. Their crown diameters were 0.8, 1.0, 1.2, 1.4, and 1.6 m, respectively, and they were selected because orchard-grown pear trees have a crown diameter range approximately between 0.8–1.6 m. The duct fan was fixed on the  $x$ -direction platform of the 3D module 0.5 m from the edge of the canopy. The airflow velocity was measured every 0.1 m along the centre of the spray direction using a TSI9545 hot-wire anemometer, starting from the outer layer of the canopy, with the first measurement taken on the outermost side of the canopy and the last at the first branch inside the canopy. Each airflow velocity was measured five times and averaged, as shown in Figure 3. The airflow velocity in the canopy was changed by adjusting the fan frequency to measure the change in airflow velocity at the edge of the canopy at 6, 9, 12, 15, and 18 m/s, respectively. Data were recorded and the above operations were carried out for the remaining four pear trees with different crown diameters under the same conditions.

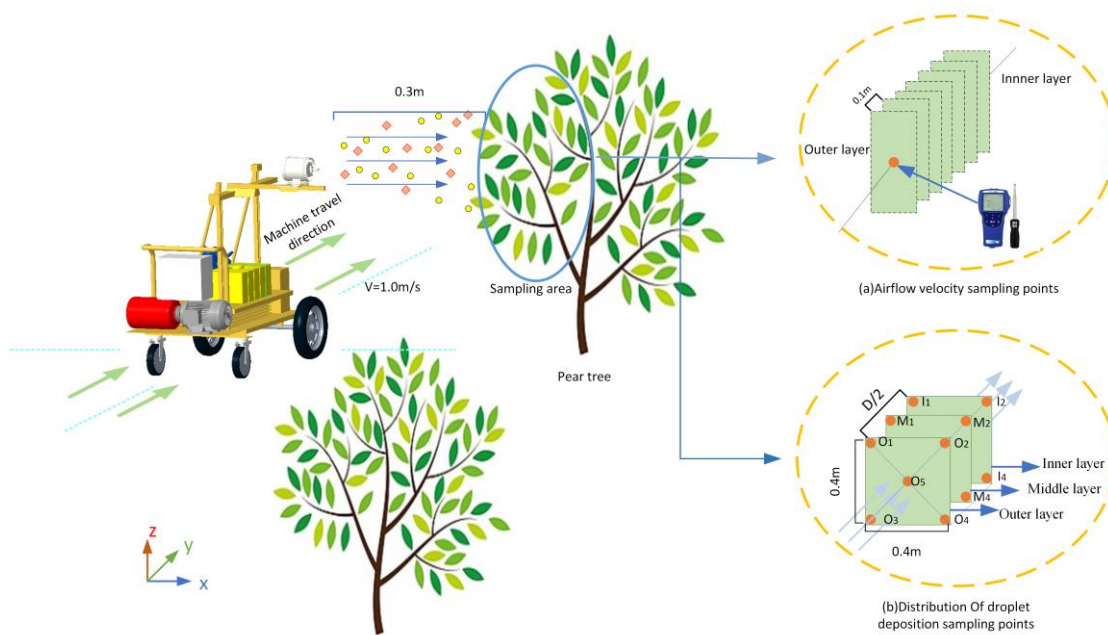


**Figure 3.** Map of airflow velocity measurement points within the pear canopy.

**2.3. Comparative Analysis of Droplet Deposition Coverage at Different Inner Canopy Airflow End Velocities**

Under the conditions described above, 90 mm diameter filter paper (Hangzhou Beimu, China) was used to collect spray droplets, and an aqueous solution of Ponceau 2R (a 5‰ highly extractable and low degradable food colour, Shanghai Dye Research Institute Co., Ltd., Shanghai, China) was selected as the tracer material. A  $76 \times 76$  mm piece of cardboard (Hangzhou, China) was used to measure droplet coverage and was fixed to the front and back surface of the pear leaf with a paper clip. Since this experiment used a single nozzle for spraying, the sampling distribution range was set according to the

effective nozzle spray range, and five sampling points were arranged as shown in Figure 3. Adjacent sampling points were 0.4 m apart horizontally and 0.4 m apart vertically. The fifth point was placed at the diagonal intersection of the remaining four points, marked as O<sub>1</sub>–O<sub>5</sub>, M<sub>1</sub>–M<sub>5</sub>, and I<sub>1</sub>–I<sub>5</sub> (O, M, and I correspond to the outer, middle, and inner layers, respectively), and the spacing of the three sampling surfaces was set as D/4 (D is the diameter of the crown).

The height of the fan was set equal to the height of the sampling centre point O<sub>5</sub> of each layer, the control spray pressure was set at a constant of 0.8 MPa, the flow rate at 50 mL/s, the distance between the nozzle and the outermost part of the pear tree at approximately 0.3 m, and the height from the ground at approximately 1.5 m. The spraying platform was driven smoothly over the target pear tree with a travel speed of 1.0 m/s, which is the conventional local orchard application travel speed, and after the experiment was finished, the cardboard and filter paper were completely dried, collected, and stored in pre-labelled plastic bags to await further processing. After adjusting the fan frequency, a total of five sets of experiments for all five pear trees were carried out under the same conditions.

#### 2.4. Validation Field Trials

Two airflow delivery scenarios were set up for comparative analysis. Scenario 1: the four airflow outlets were set to  $v_1$ ,  $v_2$ ,  $v_3$ , and  $v_4$ , respectively, which denote the outlet airflow velocity that satisfies the ICAEV. Scenario 2: the four air outlets were set to the same airflow velocity,  $v$  ( $v$  is the average of  $v_1$ ,  $v_2$ ,  $v_3$ , and  $v_4$ ). Spraying experiments were conducted at an operating speed of 1.0 m/s under these two scenarios. At the completion of each experiment, the cardboard and filter paper were dried and collected for subsequent processing.

In this experiment, a pear tree with a leaf area density of 5.20 m<sup>2</sup>/m<sup>3</sup>, an average crown diameter of 1.2 m, and a height of approximately 2.1 m was selected, and its crown diameter was 0.8, 1.2, 1.6, and 1.4 m from top to bottom (0.4 m apart), divided into A, B, C, and D layers, respectively. Nine sheets of 76 × 76 mm cardboard and 90 mm diameter filter paper were arranged in a 3 × 3 grid for each layer in the front half of the canopy along the wind direction, and a 3 m drift pole was arranged at the back, 1 m from the pear tree in the wind direction. One collection point was arranged every 15 cm from the top to the bottom of the drift pole, corresponding to K1–K15, respectively, as shown in Figure 4.

#### 2.5. Data Processing

After these field experiments were completed, the experimental samples were scanned using a high-resolution camera (MICROTEK H-Screen 701, Shanghai, China) to determine the coverage of Ponceau R2 spray droplets on the cardboard, and the resulting images were processed using grayscale binarisation and threshold division by MATLAB.

The absorbance coefficient was measured using 5‰ solution of Ponceau 2R used in the field experiment. The filter paper was cut into strips and immersed in a beaker containing 200 mL distilled water, and the shredded filter paper was completely submerged in water by stirring with a glass rod and left for 10–15 min. When the Ponceau R2 on the filter paper was completely dissolved into the water, the absorbance of the solution in the beaker was measured at 568 nm with a UV2000 spectrophotometer (UNICO Instrument Co., Ltd., Shanghai, China). The cuvette was 1 cm thick and the absorbance coefficient was 4.731 L·(g·cm)<sup>−1</sup>; the concentration of the solution was determined according to the calibration curve and the amount of spray droplets deposited on the filter paper per unit area was obtained based on Equation (1).

$$q = \frac{1000AV}{KLS} \quad (1)$$

where  $q$  is the value of Ponceau R2 deposition on the filter paper (μg/cm<sup>2</sup>),  $A$  is the absorbance value,  $V$  is the volume of distilled water (mL),  $K$  is the absorbance coefficient (L·(g·cm)<sup>−1</sup>),  $L$  is the cuvette thickness (cm), and  $S$  is the filter paper area (cm<sup>2</sup>).

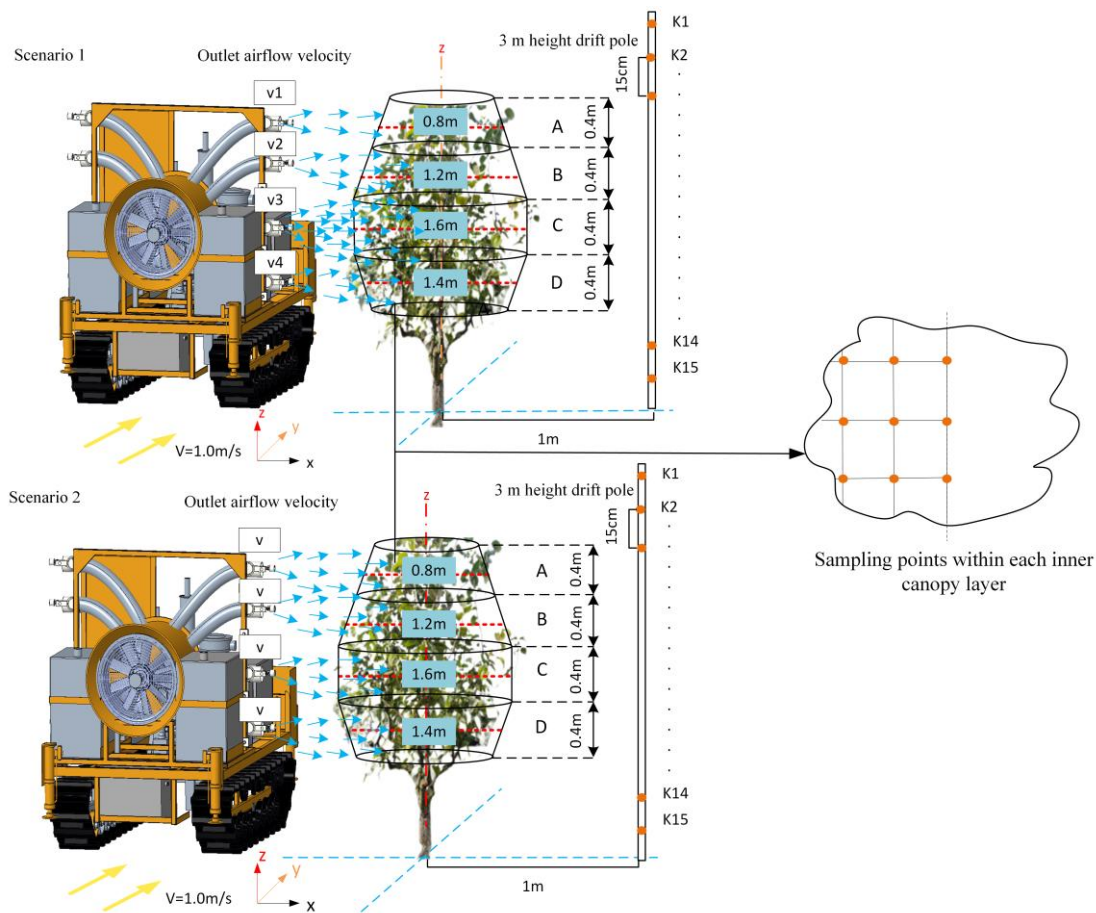


**Figure 4.** Validation field trials. Scenario 1: the four airflow outlets were set to different airflow velocities, which satisfy the ICAEV. Scenario 2: the four air outlets were set to the same airflow velocity.

After determining the Poncau R2 deposition at each sampling point, the mean  $X_i$  and the standard deviation  $S_D$  of the deposition per unit area of each layer was calculated. The coefficient of variation of the distribution of droplets in the pear canopy was calculated based on Equations (2) and (3) as follows:

$$\bar{q} = \frac{q_1 + q_1 + \dots + q_i + \dots + q_n}{n} \tag{2}$$

$$CV = \frac{S_D}{\bar{q}} \times 100\% \tag{3}$$

where  $q_i$  is the spray droplets deposited at each sampling point in each layer ( $\mu\text{g}/\text{cm}^2$ ),  $\bar{q}$  is the mean value of spray droplet deposition at sampling points in the layer ( $\mu\text{g}/\text{cm}^2$ ),  $n$  is the number of sampling points per layer within the pear canopy,  $S_D$  is the standard deviation of  $X_i$  ( $\mu\text{g}/\text{cm}^2$ ), and  $CV$  is the coefficient of variation of droplet deposition in the layer (%). The coefficient of variation of the coverage was calculated in the same way.

### 3. Results

#### 3.1. Inner Canopy Airflow Velocity Distribution

Figure 5 shows the airflow attenuation inside the pear canopy when the incoming velocity (i.e., the velocity of airflow reaching the edge of the canopy) was 6, 9, 12, 15, and 18 m/s when the crown diameter was 0.8, 1.0, 1.2, 1.4, and 1.6 m, respectively. The curve change shows that the airflow attenuated more quickly in the outer layer of the pear canopy (0–0.3 m), where the airflow velocity decay proportion was 44.33–57%, while the decay proportion at the centre (0.3 m to the innermost layer of the canopy) was <35%. When the

incoming airflow velocity was low, the curve change trend was relatively flat, whereas when the incoming airflow velocity was higher, the initial trend of the curve change was steeper. It is clear from the test results that (1) as the incoming airflow velocity increased, the degree of attenuation of airflow increased, therefore promoting the entry of spray droplets into the canopy by boosting the incoming airflow velocity. The limited, negative effects that may be caused by such an airflow velocity boost need to be considered; (2) in the five pear trees studied, the majority of airflow velocity loss occurred in the middle and outer layer of the canopy. In general, rapid airflow decay took place in the 0–0.3 m section and slow airflow decay occurred in the 0.3–0.8 m section.

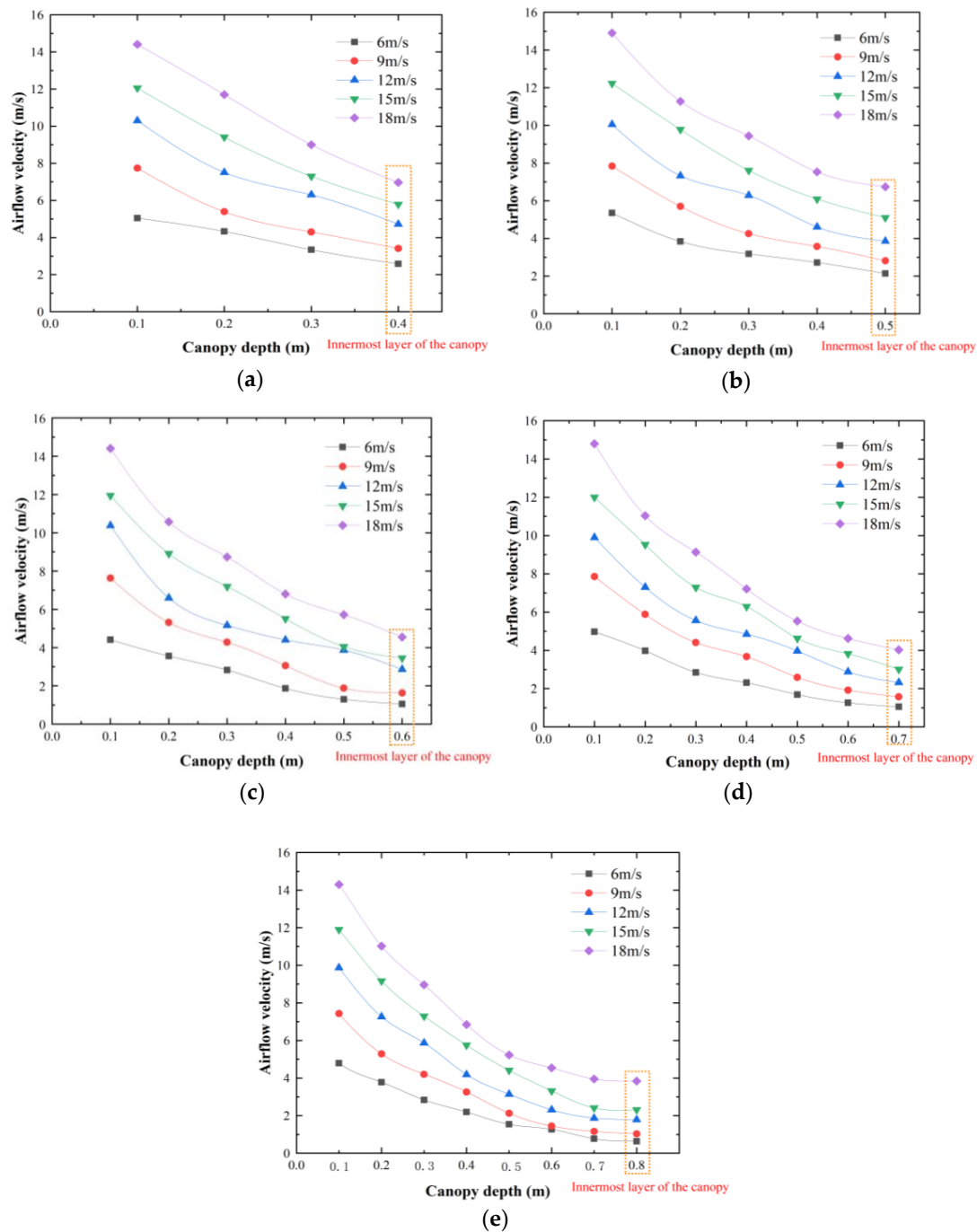


**Figure 5.** Variation in airflow attenuation within the canopy of pear trees of different crown diameters. (a) Crown diameter 0.8 m. (b) Crown diameter 1.0 m. (c) Crown diameter 1.2 m. (d) Crown diameter 1.4 m. (e) Crown diameter 1.6 m.

### 3.2. Effect of End Airflow Velocity within Various Layers of the Crown along the Direction of Airflow Delivery

Table 2 shows that when the ICAEV changed from 0.64 to 6.97 m/s, the average deposition in the outer layer decreased from a maximum of 106.26  $\mu\text{g}/\text{cm}^2$  to a minimum of 80.23  $\mu\text{g}/\text{cm}^2$ , with an average deposition decay ranging from 10–21%. The average deposition in the middle layer increased from a minimum of 24.89  $\mu\text{g}/\text{cm}^2$  to a maximum of 56.39  $\mu\text{g}/\text{cm}^2$ , with an average increase of approximately 60%. The inner layer deposition increased slightly but remained at approximately 10%. Combining the mean deposition variance and range variation, it is clear that an increase in the ICAEV narrowed the interlayer gap in application volume in the direction of airflow delivery. The mean overall deposition variance and range difference gradually increased with increasing crown diameter, indicating that the uniformity of droplet distribution was also influenced by crown diameter.

**Table 2.** Distribution of spray droplet deposition in the crown.

ICAEV (m/s)	Average Deposition ( $\mu\text{g}/\text{cm}^2$ )			Range	Variance	
	Outer Layer	Middle Layer	Inner Layer			
0.8 m	2.58	96.86	32.00	13.49	83.37	1277.78
	3.41	87.22	36.64	16.50	70.72	885.03
	4.72	86.26	46.92	15.80	70.46	831.19
	5.79	84.41	52.92	15.76	68.65	787.26
	6.97	81.44	52.32	15.17	66.27	735.53
1.0 m	2.14	92.46	29.43	11.06	81.40	1215.13
	2.81	91.20	36.06	12.75	78.45	1082.02
	3.86	88.01	43.75	11.21	76.80	990.67
	5.10	82.95	47.90	11.82	71.13	843.31
	6.32	80.23	43.91	10.76	69.47	804.91
1.2 m	1.29	96.40	32.45	10.42	85.98	1329.72
	1.83	93.49	39.85	11.47	82.02	1156.66
	2.86	86.69	42.61	12.58	74.11	926.35
	3.45	85.46	42.77	11.57	73.89	917.29
	5.01	84.68	47.88	11.26	73.42	898.42
1.4 m	1.05	106.26	34.70	6.79	99.47	1754.90
	1.57	91.50	48.14	7.31	84.19	1181.68
	2.32	86.91	51.02	9.89	77.02	990.21
	3.01	83.95	56.31	10.01	73.94	930.53
	4.03	83.82	56.39	10.16	73.66	923.93
1.6 m	0.64	101.23	24.89	3.56	97.67	1750.41
	1.03	95.78	25.52	5.14	90.64	1514.56
	1.79	88.19	33.02	6.21	81.98	1164.80
	2.31	88.56	46.44	6.71	81.85	1116.89
	3.84	81.38	52.70	6.93	74.45	940.03

### 3.3. Effect of Canopy End Airflow Velocity on Droplet Deposition

To investigate the effect of pesticide delivery to the inner canopy, we examined the average deposition (AD), the average coverage (AC), the average deposition in the inner layer (ADI), the average abaxial coverage of the inner layer leaves (AACI), the coefficient of variation of the inner layer coverage (CVIC), and the coefficient of variation of the inner layer deposition (CVID), which were used to evaluate the effect of spray droplet deposition under different conditions. Among these, the CVIC and CVID were considered inverse indicators. Figure 6 shows the variation curves of six indicators for five pear tree canopy sizes with different ICAEVs, and Figure 7 shows the actual spraying application on sampling filter paper and cardboard.

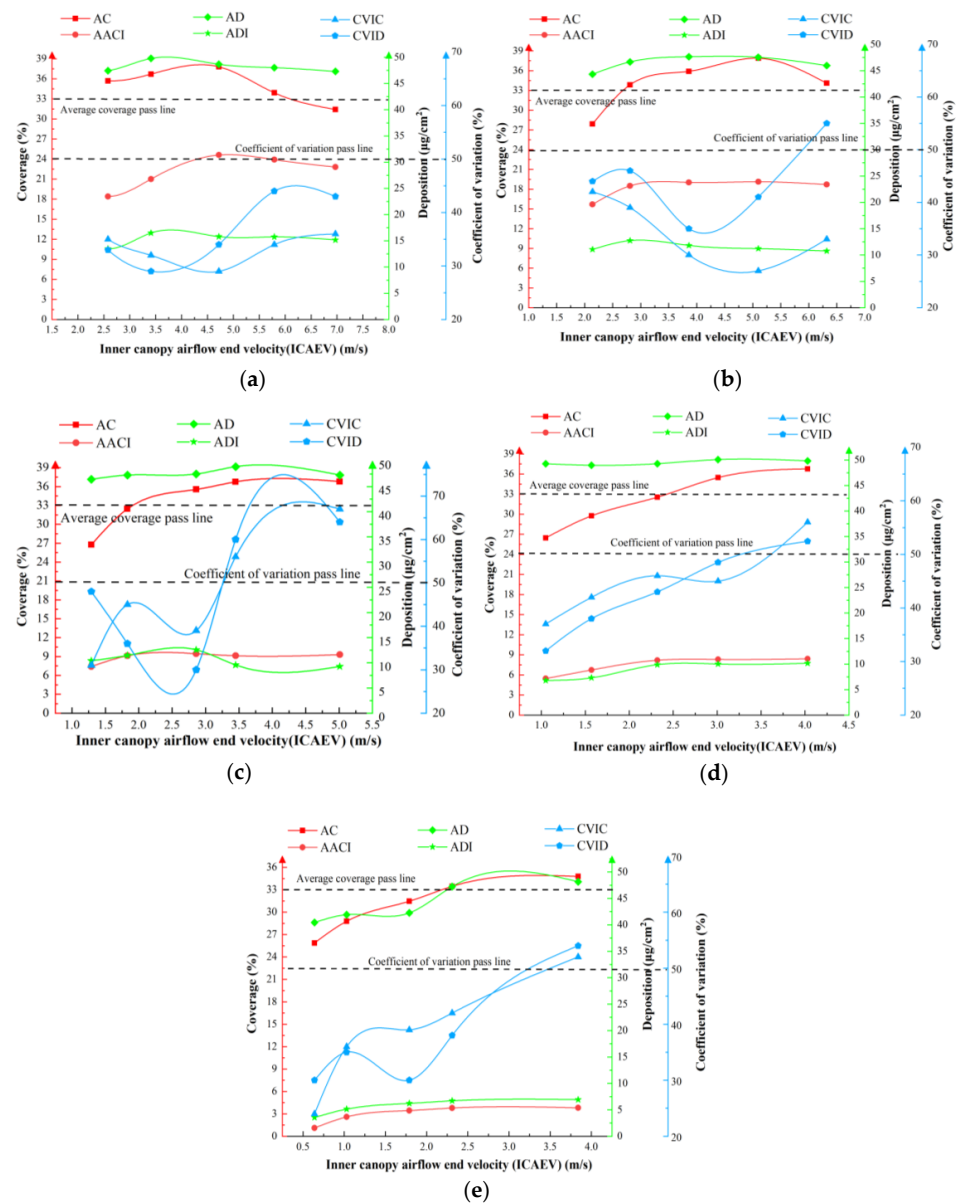


**Figure 6.** Variation curves of six indicators of pear trees with five canopy sizes under different inner canopy airflow end velocity. (a) Crown diameter 0.8 m. (b) Crown diameter 1.0 m. (c) Crown diameter 1.2 m. (d) Crown diameter 1.4 m. (e) Crown diameter 1.6 m.



**Figure 7.** Detection of spray droplet coverage and deposition in the inner canopy. (a) Filter paper to detect droplet. (b) Cardboard to detect coverage.

As shown in Figure 6a–c, the AD was close to the deposition threshold of  $50 \mu\text{g}/\text{cm}^2$  for crown diameters of 0.8–1.2 m with an ICAEV of 3.5–4.0 m/s and for crown diameters of 1.4–1.6 m with an ICAEV of 3.25 m/s. This implies that a continuous increase in the ICAEV did not significantly increase deposition past a certain threshold value.

The CVIC and CVID decreased when the ICAEV continued to increase to a certain value. For example, when the pear tree crown diameter was 1.2 m and the ICAEV increased to 3.25 m/s, the deposition of local droplets in the same layer increased, and the CVID exceeded 50% and gradually increased, at which time the uniformity of deposition decreased. As the high-speed airflow was more capable of blowing open the branches and leaves and forming airflow channels within the canopy; it also meant that the airflow could not be dispersed. Meanwhile, the high-speed airflow caused stronger disturbance of the branches and leaves and the droplets could be flung off after deposition, forming excess local deposition. Related studies [25,26] also concluded that excessively high-speed airflow caused droplet loss, and that reasonable inner canopy airflow end velocity is crucial.

Comparing the AC curve with the AD curve reveals that the variation in the ICAEV had a greater influence on coverage than deposition. In Figure 6a–e for different crown diameters, the overall AD varied between 5 and  $8 \mu\text{g}/\text{cm}^2$ , and the overall AC varied between 7 and 12%. Considering that the actual average inner AD and AC varied above and below the benchmarks of  $46 \mu\text{g}/\text{cm}^2$  and 33%, respectively, we concluded that the actual effect of ICAEV variation on coverage was significantly greater than that on deposition.

### 3.4. Proposal of Suitable Canopy End Airflow Velocity in Pear Trees

Of all the evaluation indices, the higher the AC, AACI, AD, and ADI, the better the application. Conversely, the lower the CVIC and CVID, the better the application. Combined with the requirements in the “Operational quality of air-assisted orchard sprayers (NY/T992-2006)” airflow delivery standard [27]—(1)  $\text{CVID} \leq 50$ , (2) the adhesion rate of the pesticide on the crop is at least 33%—the suitable ICAEV is 2.70–3.18 m/s, as shown in Figure 8.

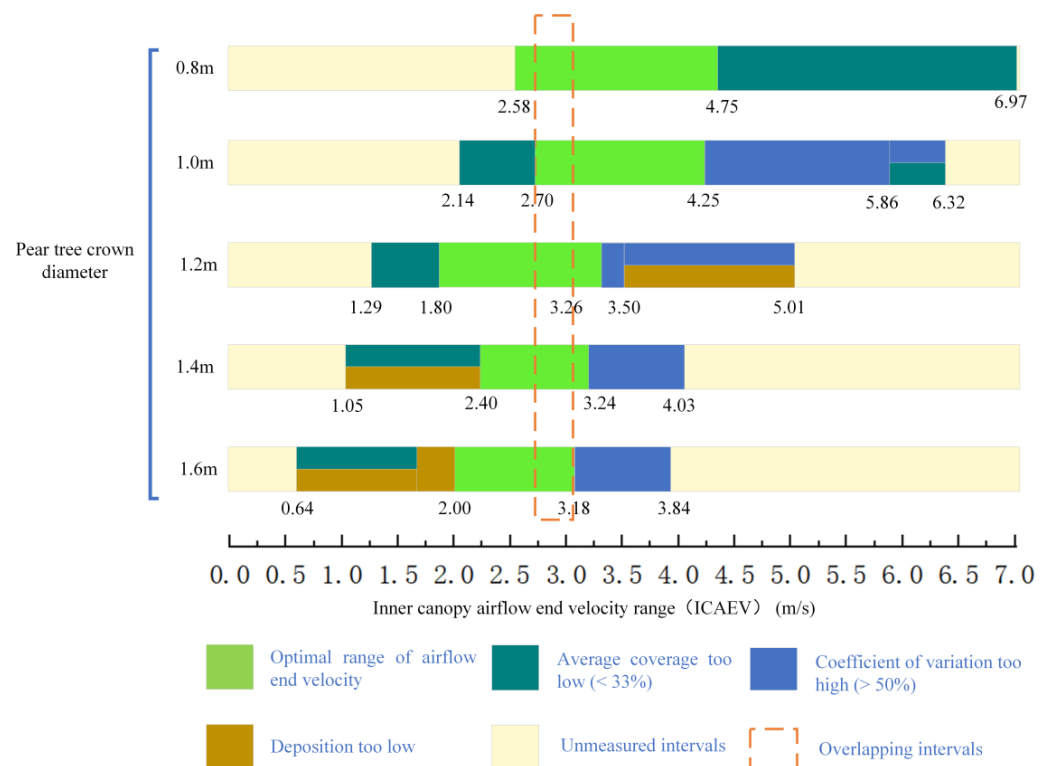


**Figure 8.** Corresponding suitable inner canopy airflow end velocity intervals for different crown diameters.

### 3.5. Field Validation Trials

The corresponding outlet airflow velocities for each layer in Scenario 1 were 7.88, 11.07, 16.54, and 13.67 m/s, respectively; the same outlet airflow velocity (12.29 m/s) was used for Scenario 2. Figure 9 shows that the overall AC of droplets in Scenarios 1 and 2 were 37.91 and 34.05%, respectively; the AD values were 45.5 and 41.88  $\mu\text{g}/\text{cm}^2$ , respectively. However, these values were not significantly different. Further, the AC and AD of the C layer in Scenario 1 were significantly higher than those in Scenario 2, mainly due to the larger outlet airflow velocity corresponding to C layers of the crown diameter, and the ICAEV at this velocity condition is suitable. In contrast, the airflow velocity at each outlet in Scenario 2 was uniform, and the ICAEV in the layer with a larger crown diameter might not achieve the effect in Scenario 1. Overall, the spatial variation distribution of airflow formed by uniform airflow delivery application is of great significance in the case of irregular canopies. The coefficient of variation of deposition (CVD) also verified the significance of non-uniform airflow delivery application based on suitable ICAEV. The coefficients of variation for Scenarios 1 and 2 were 42.25 and 51.25%, respectively, because the spray deposition in the C layers with larger canopy diameters was significantly different in the two scenarios.

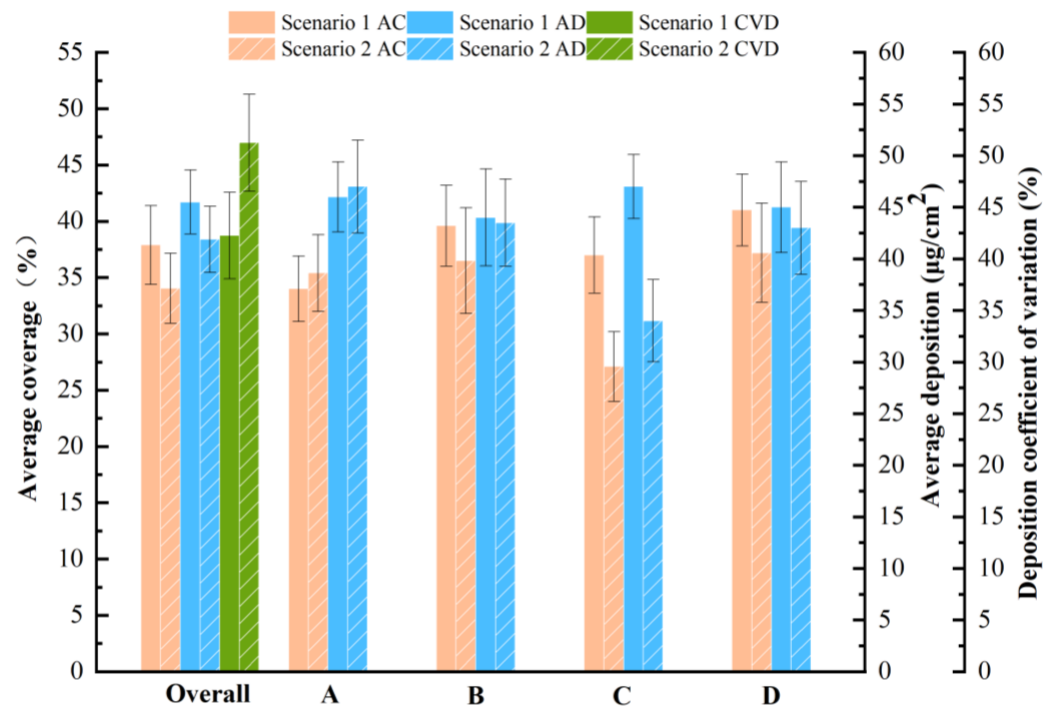


**Figure 9.** Comparative analysis of the effects of the two application scenarios.

Table 3 shows that the drift in Scenario 1 was 12.59  $\mu\text{g}/\text{cm}^2$  less than that of Scenario 2. In Scenario 1 segments  $K_1$ – $K_5$ , the drift was 6.14  $\mu\text{g}/\text{cm}^2$ , i.e., 9.19  $\mu\text{g}/\text{cm}^2$  less than that of Scenario 2; the drift in  $K_6$ – $K_{10}$  was 8.76  $\mu\text{g}/\text{cm}^2$ , 1.38  $\mu\text{g}/\text{cm}^2$  less than that of Scenario 2; and the drift in  $K_{11}$ – $K_{15}$  was 9.43  $\mu\text{g}/\text{cm}^2$ , 2.02  $\mu\text{g}/\text{cm}^2$  less than that of Scenario 2. Since the drift in the  $K_1$ – $K_5$  segment corresponds to the A layer of the canopy, it requires lower airflow velocities due to the smaller canopy diameter. Another phenomenon caused by the continuous increase in airflow after deposition had reached the saturation threshold is the increase in drift. Therefore, in order to reduce drift, it is critical to set the outlet airflow velocity in accordance with the smaller crown diameter, based on the suitable ICAEV.

**Table 3.** Droplet drift under two application scenarios.

Average Drift of Droplets ( $\mu\text{g}/\text{cm}^2$ )	K1–K5	K6–K10	K11–K15	Overall
Scenario 1	$6.14 \pm 1.76$	$8.76 \pm 2.18$	$9.43 \pm 2.04$	$24.33 \pm 3.64$
Scenario 2	$15.33 \pm 3.58$	$10.14 \pm 2.23$	$11.45 \pm 2.18$	$36.92 \pm 4.26$

#### 4. Discussion

At present, research on airflow in air-assisted applications mainly falls into two major categories: sprayers for the outside of the canopy and airflow interaction inside the canopy. The former is mainly based on the classical turbulent jet theory [28,29] and the shape structure of crop growth to ensure that the droplets reach the outside of the canopy with a certain initial velocity, and redesigning spraying equipment to achieve better application. The latter mainly studies the porosity and closure within the canopy [30] and discusses the air and mist flow inside the crown.

The impact of airflow velocity on actual application is limited, and the search for reasonable airflow velocity is a major concern when designing sprayers [31–34]. Researchers have two main objectives when designing plant protection air-assisted spraying systems: (1) to design different air-assisted sprayer systems based on various canopy structures to achieve full coverage and less drift of the aerosol stream, for example, adopting stacked fans [35] and adjusting the wind baffle [36] or the angle of the airflow outlet [8] to achieve the rationalisation of air and mist flow field distribution; (2) adjusting the airflow velocity in order to achieve high penetration of air and spray based on differing canopy biomasses. Air velocity is generally regulated by adjusting the area of the air outlet and inlet [37,38] or the fan speed [39,40]. Reasonable air velocity is often verified by measuring droplet deposition coverage. The airflow velocity value of interest is usually the outlet airflow velocity or the airflow velocity reaching the edge of the canopy [41–43]. The canopy, as an operational target, is also an important factor in airflow attenuation. It is not always clear which air velocity is needed to reach the inner layer of the canopy.

To identify the suitable ICAEV, we first analysed the inner canopy airflow velocity under different conditions. The airflow attenuation in the 0–0.3 m section of the pear tree canopy ranged from 44.33 to 57%, and the attenuation at 0.3 m to the innermost canopy was <35%. Based on Walklate et al. (1996) [22] and Farooq et al. (2004) [44], who theorised that the airflow velocity in the canopy decays exponentially with increasing canopy penetration distance, we clarified that the inflection point of airflow decay in the pear tree was 0.3 m into the canopy. Previous studies demonstrated that the amount of deposition of the chemical solution eventually reaches a threshold value with variations in the outlet airflow velocity [45]; we explained this from the perspective of the ICAEV. As our focus is on the effect of application in the inner canopy, the proposed suitable ICAEV for pears was supported by the addition of the ADI, the AACI, the CVIC, and the CVID as well as examining the AC and AD.

In this study, the suitable ICAEV was obtained for one variety of pear tree and field validation experiments were conducted to provide reference for similar studies on other types of fruit trees or crops. Since a single species was selected for the experiment, a fruiting pear tree, fruit trees of different growth periods have not been studied. The petiole force and the resulting resistance to inner canopy airflow of fruit trees at different periods are also different, and further research is needed to study the effect of fruit tree growth period on the ICAEV. In the future, the conditions of airflow kinetic energy required for effective deposition could also be analysed from the perspective of branch and leaf disturbance under the action of airflow.

#### 5. Conclusions

- (1) Incoming air velocity and pear crown diameter are important factors affecting the ICAEV. The airflow decayed faster at 0–0.3 m in the outer layer of the canopy, with

the airflow velocity decay ratio ranging from 44.33 to 57%, while the decay ratio at 0.3 m to the innermost layer of the canopy was <35%. Therefore, for the airflow to reach the inner canopy and maintain a certain velocity, it is necessary to increase the initial incoming velocity or reduce the resistance of the airflow in the outer canopy.

- (2) A sustained increase in the ICAEV does not produce a significant elevation in deposition once it has gradually increased and reached a certain threshold value. The CVIV and CVID decreased when the ICAEV continued to increase until a certain value. By examining the indexes of AC, AD, and ADI, as well as AACI and the CVIC and CVID, and combining these with the operational quality requirements of the air-assisted orchard sprayer, the suitable range of the end velocity of inner canopy airflow was set at 2.70 to 3.18 m/s.
- (3) Using an application method suitable for the ICAEV, the deposition of droplets in the lower and middle layers of the larger crown diameter was significantly higher, which also effectively improved the overall deposition uniformity and reduced the droplet drift by 12.59  $\mu\text{g}/\text{cm}^2$ .

**Author Contributions:** R.S. and H.S. performed the experiment; R.S. and W.Q. wrote the manuscript and analysed the data; F.A. and W.Q. suggested changes to the article; R.S., Z.Z. processed the data and the field test; X.L., H.Y., and J.G. contributed to the concept of the study. All authors have read and agreed to the published version of the manuscript.

**Funding:** This work was co-financed by the National Natural Science Foundation of China (Grant No. 32171905) and the Jiangsu Agricultural Science and Technology Innovation Fund (CX203172).

**Data Availability Statement:** Not applicable.

**Conflicts of Interest:** The authors declare no conflict of interest.

## References

1. Pan, X.L.; Dong, F.S.; Wu, X.H.; Xu, J.; Liu, X.G.; Zheng, Y.Q. Progress of the discovery, application, and control technologies of chemical pesticides in China. *J. Integr. Agric.* **2019**, *18*, 840–853. [[CrossRef](#)]
2. Chen, B.T.; Zheng, Y.J.; Jiang, S.J.; Yang, S.H.; Lv, H.T.; Kang, F. Resource Consumption Evaluation Model of Orchard Spray Machinery. *Trans. Chin. Soc. Agric. Mach.* **2020**, *51*, 289–297.
3. Rathnayake, A.P.; Khot, L.R.; Hoheisel, G.A.; Thistle, H.W.; Teske, M.E.; Willett, M.J. Downwind spray drift assessment for airblast sprayer applications in a modern apple orchard system. *Trans. ASABE* **2021**, *64*, 601–613. [[CrossRef](#)]
4. Wang, S.L.; Fan, D.Q.; Li, X.; Zhou, H.; Zhang, M.N.; Yan, T.T.; Lu, X.L. Effect of Orchard Sprayers on Dermal Exposure of Operators. *J. Ecol. Rural Environ.* **2020**, *36*, 1612–1618.
5. Gu, C.C.; Liu, Z.J.; Pan, G.T.; Pu, Y.J.; Yang, F.Z. Optimization of working parameters for 3MGY-200 axial air-assisted sprayer in kiwifruit orchards. *Int. J. Agric. Biol. Eng.* **2020**, *13*, 81–91. [[CrossRef](#)]
6. Qiu, W.; Sun, H.; Sun, Y.H.; Liao, Y.Y.; Zhou, L.F.; Wen, Z.J. Design and test of circulating air-assisted sprayer for dwarfed orchard. *Trans. Chin. Soc. Agric. Eng.* **2021**, *37*, 18–25.
7. Wen, Z.J.; Qiu, W.; Zhang, Z.T.; Ding, W.M.; Lyu, X.L.; Ahmad, F.; Wang, H. Tunnel-convective air-assisted spraying technology for improving droplet deposition on hedgerow vines. *Int. J. Agric. Biol. Eng.* **2021**, *14*, 9–18. [[CrossRef](#)]
8. Qiu, W.; Li, X.L.; Li, C.C.; Ding, W.M.; Lv, X.L.; Liu, Y.D. Design and test of a novel crawler-type multi-channel air-assisted orchard sprayer. *Int. J. Agric. Biol. Eng.* **2020**, *13*, 60–67. [[CrossRef](#)]
9. Blanco, M.N.; Fenske, R.A.; Kasner, E.J.; Yost, M.G.; Seto, E.; Austin, E. Real Time Monitoring of Spray Drift from Three Different Orchard Sprayers. *Chemosphere* **2019**, *222*, 46–55. [[CrossRef](#)] [[PubMed](#)]
10. Fan, G.J.; Wang, S.Y.; Bai, P.; Wang, D.W.; Shi, W.J.; Niu, C.Q. Research on Droplets Deposition Characteristics of Anti-Drift Spray Device with Multi-Airflow Synergy Based on CFD Simulation. *Appl. Sci.* **2022**, *12*, 7082. [[CrossRef](#)]
11. Hong, S.W.; Zhao, L.Y.; Zhu, H.P. CFD simulation of airflow inside tree canopies discharged from air-assisted sprayers. *Comput. Electron. Agric.* **2018**, *149*, 121–132. [[CrossRef](#)]
12. Chen, R.K. *Study on the Change of Canopy Porosity of High Depression Crops under the Action of Auxiliary Airflow*; Shandong Agricultural University: Taian, China, 2017.
13. Liu, X.H. *Research on the Penetration Law of Wind-Fed Fog Droplets within the Depressed Canopy Based on Stratified Porosity*; Shandong Agricultural University: Taian, China, 2021.
14. Liu, C.C.; Zheng, Z.Q.; Cheng, H.; Zou, X.Y. Airflow around single and multiple plants. *Agriv. For. Meteorol.* **2018**, *252*, 27–38. [[CrossRef](#)]
15. Zhu, Y.Z.; Guo, Q.W.; Tang, Y.; Zhu, X.; He, Y.; Huang, H.S.; Luo, S.M. CFD simulation and measurement of the downwash airflow of a quadrotor plant protection UAV during operation. *Comput. Electron. Agric.* **2022**, *201*, 107286. [[CrossRef](#)]

16. Zhang, H.; Qi, L.; Wan, J.; Musiu, E.M.; Zhou, J.; Lu, Z.; Wang, P. Numerical simulation of downwash airflow distribution inside tree canopies of an apple orchard from a multirotor unmanned aerial vehicle (UAV) sprayer. *Comput. Electron. Agric.* **2022**, *195*, 106817. [[CrossRef](#)]
17. Duga, A.T.; Delele, M.A.; Ruysen, K.; Dekeyser, D.; Nuyttens, D.; Bylemans, D.; Nicolai, B.M.; Verboven, P. Development and validation of a 3D CFD model of drift and its application to air-assisted orchard sprayers. *Biosyst. Eng.* **2017**, *154*, 62–75. [[CrossRef](#)]
18. Lv, X.L.; Zhang, M.N.; Chang, Y.H.; Lei, X.H.; Yang, Q.S. Influence of deflector angles for orchard air-assisted sprayer on 3D airflow distribution. *Trans. Chin. Soc. Agric. Eng.* **2017**, *33*, 81–87.
19. Chen, J.Z.; Song, S.R.; Sun, D.Z.; Hong, T.S.; Zhang, L. Test on airflow field and spray characteristics for long-range air-blast sprayer. *Trans. Chin. Soc. Agric. Eng.* **2017**, *33*, 72–79.
20. Grella, M.; Marucco, P.; Zwervaegher, I.; Gioelli, F.; Bozzer, C.; Biglia, A.; Manzone, M.; Caffini, A.; Fountas, S.; Nuyttens, D. The effect of fan setting, air-conveyor orientation and nozzle configuration on airblast sprayer efficiency: Insights relevant to trellised vineyards. *Crop Prot.* **2022**, *155*, 105921. [[CrossRef](#)]
21. Qiu, W.; Guo, H.B.; Cao, Y.B.; Li, X.L.; Wu, J.H.; Chen, Y.F.; Yu, H.F.; Zhang, Z.W. An electrical vortex air-assisted spraying system for improving droplet deposition on rice. *Pest Manag. Sci.* **2022**, *78*, 4037–4047. [[CrossRef](#)]
22. Walklate, P.; Weiner, K.-L.; Parkin, C. Analysis of and experimental measurements made on a moving air-assisted sprayer with two-dimensional air-jets penetrating a uniform crop canopy. *J. Agric. Eng. Res.* **1996**, *63*, 365–377. [[CrossRef](#)]
23. Li, J.; He, M.X.; Cui, H.J.; Lin, P.Y.; Chen, Y.Y.; Ling, G.X.; Huang, G.W.; Fu, H. Characterizing Droplet Retention in Fruit Tree Canopies for Air-Assisted Spraying. *Agriculture* **2022**, *12*, 1093. [[CrossRef](#)]
24. Chao, X.Y.; Chen, S.; Qiu, W.; Lv, X.L.; Li, H.; Han, C.J.; Ahmad, F. Simulation and Validation of the Air Flow Generated by a Multi-channel Air Assisted Sprayer. *IEEE Access* **2019**, *7*, 94848–94857. [[CrossRef](#)]
25. Xi, T.; Li, C.; Qiu, W.; Wang, H.; Lv, X.; Han, C.; Ahmad, F. Droplet Deposition Behavior on a Pear Leaf Surface under Wind-Induced Vibration. *Applied Engineering in Agriculture* **2020**, *36*, 913–926. [[CrossRef](#)]
26. Li, Z. *Wind-Induced Trees Vibration Simulation on Different Canopy Structure*; Fuzhou University: Fuzhou, China, 2016.
27. *NY/T 650-2013*; Operational quality of sprayers. Ministry of Agriculture of the People’s Republic of China: Beijing, China, 2013; ICS 65.060.
28. Randall, J.M. The relationships between air volume and pressure on spray distribution in fruit trees. *J. Agric. Eng. Res.* **1971**, *16*, 1–31. [[CrossRef](#)]
29. Fox, R.D.; Brazee, R.D.; Reichard, D.L. A Model Study of the Effect of Wind on Air Sprayer Jets. *Trans. ASAE* **1985**, *28*, 83–88. [[CrossRef](#)]
30. Liu, X.M.; Song, L.Q.; Cui, H.Y.; Liu, Y.C.; Liu, X.H.; Wu, M.Q. Decoupling the effects of aerosol droplet stress and canopy porosity changes on deposition performance. *Journal of Agricultural Machinery* **2021**, *52*, 117–126+137.
31. Marshall, J.; Mcmechan, A.D.; Williams, K. *Low-Volume Air-Blast Spraying in British Columbia Orchards 1957–1962*; Agriculture and Agri-Food Canada: Ottawa, Canada, 2002.
32. Matthews, G.; Bateman, R.; Miller, P. *Pesticide Application Methods*; John Wiley & Sons: Hoboken, NJ, USA, 2014.
33. Landers, A. Drift from fruit sprayers-why not prevent it at source? *Asp. Appl. Biol.* **2011**, *114*, 235–242.
34. Cerruto, E. Further studies on the variation of spray deposits in vineyards with airflow rate and volume rate. *Journal of Agricultural Engineering* **2007**, *38*, 31–38. [[CrossRef](#)]
35. Godyn, A.; Holownicki, R.; Doruchowski, G.; Swiechowski, W. Dual-fan Orchard Sprayer with Reversed Air-stream-Preliminary Trials. *Agric. Eng. Int. CIGR J.* **2008**.
36. Dekeyser, D.; Duga, A.T.; Verboven, P.; Endalew, A.M.; Hendrickx, N.; Nuyttens, D. Assessment of orchard sprayers using laboratory experiments and computational fluid dynamics modelling. *Biosyst. Eng.* **2013**, *114*, 157–169. [[CrossRef](#)]
37. Pascuzzi, S. The effects of the forward speed and air volume of an air-assisted sprayer on spray deposition in tendone trained vineyards. *J. Agric. Eng.* **2013**, *44*, e18. [[CrossRef](#)]
38. Doruchowski, G.; Holownicki, R. Environmentally friendly spray techniques for tree crops. *Crop Prot.* **2000**, *19*, 617–622. [[CrossRef](#)]
39. Li, L.; He, X.; Song, J.; etc. Design and experiment of variable rate orchard sprayer based on laser scanning sensor. *Int. J. Agric. Biol. Eng.* **2018**, *11*, 101–108. [[CrossRef](#)]
40. Garcia-Ramos, F.J.; Vidal, M.; Bone, A. Field Evaluation of an Air-Assisted Sprayer Equipped with Two Reversed Rotation Fans. *Appl. Eng. Agric.* **2009**, *25*, 481–494. [[CrossRef](#)]
41. Darvishvand, M.; Brown, R.B. Performance of an air-assist forestry boom sprayer. *Can. Agric. Eng.* **1997**, *39*, 281–287.
42. Li, J.; Cui, H.; Ma, Y.; Xun, L.; Li, Z.; Yang, Z.; Lu, H. Orchard spray study: A prediction model of droplet deposition states on leaf surfaces. *Agronomy* **2020**, *10*, 747. [[CrossRef](#)]
43. Salcedo, R.; Fonte, A.; Grella, M.; Garcerá, C.; Chueca, P. Blade pitch and air-outlet width effects on the airflow generated by an airblast sprayer with wireless remote-controlled axial fan. *Comput. Electron. Agric.* **2021**, *190*, 106428. [[CrossRef](#)]
44. Farooq, M.; Salyani, M. Modeling of spray penetration and deposition on citrus tree canopies. *Trans. ASAE* **2004**, *47*, 619–627. [[CrossRef](#)]
45. Musiu, E.M.; Qi, L.; Wu, Y. Spray deposition and distribution on the targets and losses to the ground as affected by application volume rate, airflow rate and target position. *Crop Prot.* **2019**, *116*, 170–180. [[CrossRef](#)]